Seismic Behavior and Design of Unbonded Post-Tensioned Precast Concrete Walls

Yahya Kurama, Ph.D.
Assistant Professor
Department of Civil Engineering and Geological Sciences
University of Notre Dame
Notre Dame, Indiana

Stephen Pessiki, Ph.D.
Associate Professor
Department of Civil and Environmental Engineering
Lehigh University
Bethlehem, Pennsylvania

Richard Sause, Ph.D., P.E.
Associate Professor
Department of Civil and Environmental Engineering
Lehigh University
Bethlehem, Pennsylvania

Le-Wu Lu, Ph.D.
Professor
Department of Civil and Environmental Engineering
Lehigh University
Bethlehem, Pennsylvania

Unbonded post-tensioned precast concrete walls are constructed by post-tensioning precast wall panels across horizontal joints using post-tensioning steel which is not bonded to the concrete. This paper describes an analytical investigation of the seismic behavior and design of these walls. Unbonded post-tensioned precast walls with strength and initial stiffness similar to monolithic cast-in-place concrete walls can be designed to soften and undergo large nonlinear lateral drift with little damage. The nonlinear behavior is primarily due to the opening of gaps along the horizontal joints. A performance-based seismic design approach is proposed in which the walls are required to resist design level ground motions with little damage and severe survival level ground motions with damage but without failure. Shear slip along the horizontal joints is prevented by design. Nonlinear dynamic analyses show that, compared to cast-in-place walls, unbonded post-tensioned precast walls undergo larger drift, but accumulate significantly smaller residual drift during an earthquake.

The use of precast concrete walls as primary lateral load resisting systems in seismic regions is constrained by current building codes in the United States, which require that these walls emulate the behavior of monolithic cast-in-place reinforced concrete walls. However, field studies after previous earthquakes and experimental evidence[1-3] have revealed that significant damage occurs in precast walls which emulate cast-in-place walls. Moreover, precast walls which emulate cast-in-place walls do not have all of the economic advantages of precast con-

crete construction due to the use of steel and/or cast-in-place concrete components in their joints. This paper summarizes recent research at Lehigh University on the use of unbonded post-tensioned precast walls as a primary lateral load resisting system in high and moderate seismic regions.

Unbonded post-tensioned precast walls are constructed by post-tensioning precast wall panels across horizontal joints at the floor levels using post-tensioning steel which is not bonded to the concrete (Fig. 1). Dry-pack or grout may be used between the panels for alignment and for construction tolerances. These walls do not emulate the behavior of cast-in-place concrete walls. The lateral load resistance is provided by high-strength post-tensioning steel bars or multi-strand tendons, located inside ducts which are not grouted. Spiral reinforcing steel is used to confine the concrete in the wall panels near the base of the wall. Wire mesh is used as bonded reinforcement in the panels.

The research summarized in this paper is part of the PREcast Seismic Structural Systems (PRESSS) research program.[4] The research, presented in more detail by Kurama et al.,[5,6] has the ultimate goal of developing seismic building code specifications for precast walls comparable to specifications available for cast-in-place walls.

This paper shows that unbonded post-tensioned precast walls offer many significant advantages as primary lateral load resisting systems without emulating cast-in-place concrete walls, and proposes a performance-based seismic design approach for the walls. The proposed design approach can be easily incorporated into current seismic building code specifications.

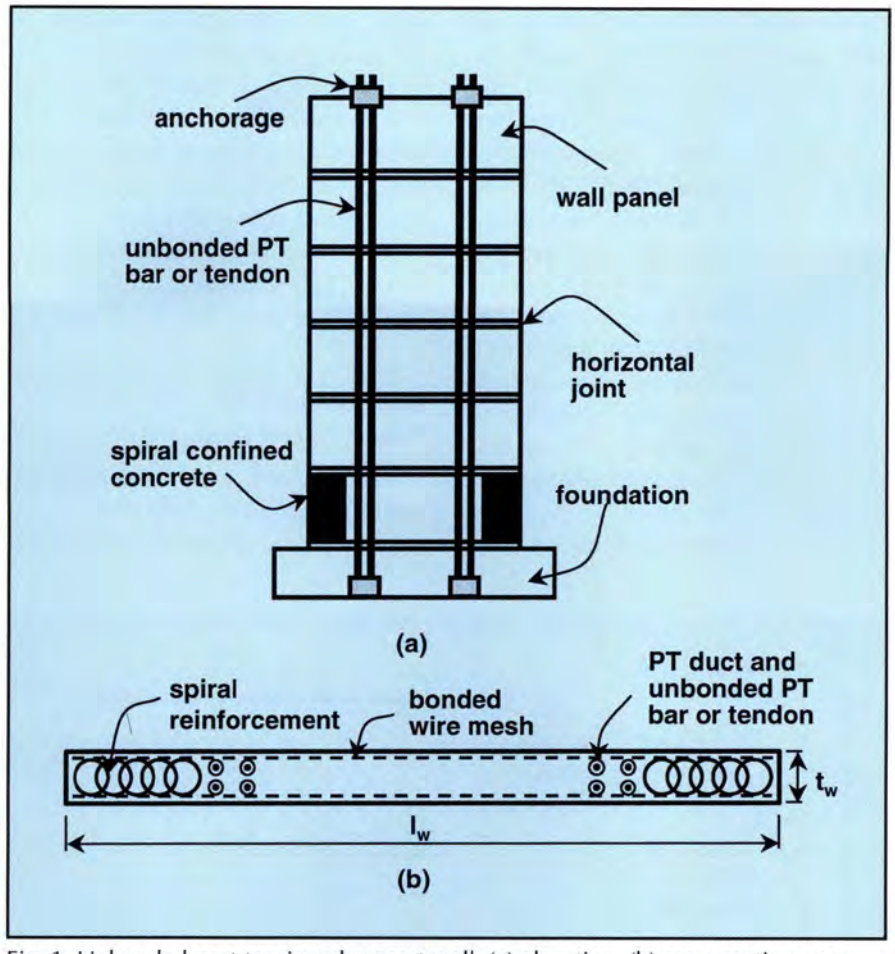

Fig. 1. Unbonded post-tensioned precast wall: (a) elevation; (b) cross section near base (enlarged).

BEHAVIOR UNDER LATERAL LOAD

The behavior of an unbonded post-tensioned precast wall under lateral load is governed by the behavior along the horizontal joints. Fig. 2 shows the two types of behavior that can occur along the joints, namely, gap opening and shear slip. In the case of gap opening, the post-tensioning force and the axial force due to gravity load provide a restoring force that tends to close the gaps upon unloading.

In the case of shear slip, however, there is no restoring force to reverse the slip. Thus, it is difficult to control the magnitude of the shear slip displacements which may occur during an earthquake. Shear slip should be prevented by proper design and detailing of the wall.

An analytical model based on fiber beam-column elements was developed to investigate the behavior of walls which are designed to have a gap opening along the joints but not shear slip.[5] A significant advantage of using fiber elements is that a reasonably ac-

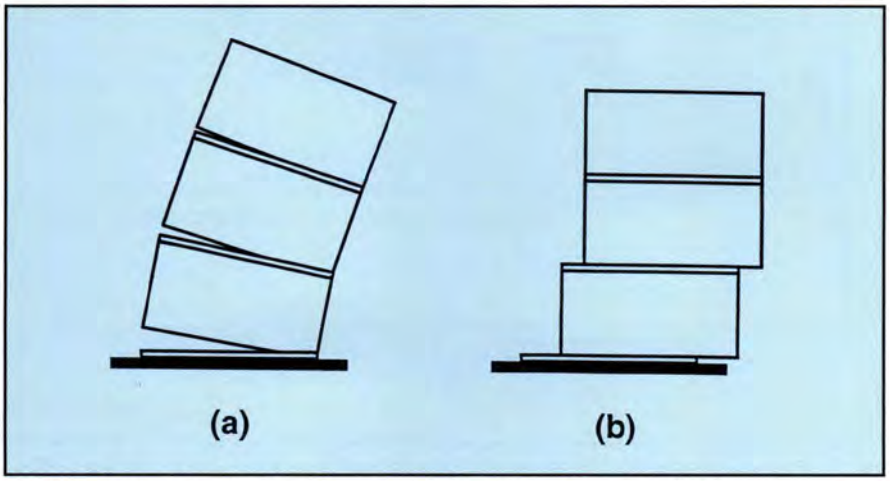

Fig. 2. Behavior of wall along horizontal joints: (a) gap opening; (b) shear slip.

curate model can be developed using only uniaxial stress-strain models for concrete and post-tensioning steel, and the dimensions of the wall. The fiber wall model accounts for axial-flexural interaction, hysteretic behavior of the post-tensioning steel and concrete including crushing of concrete, and gap opening along the joints.

Comparisons of analysis results obtained using the fiber wall model with results obtained using finite element models which use contact elements to model the gap opening indicate that the fiber wall model is capable of predicting both the global (e.g., base-shear-roof-drift) behavior and the local (e.g., gap opening) behavior of the walls reasonably well.[7]

The fiber wall model was used to conduct nonlinear static lateral load analyses and nonlinear dynamic time-history analyses of prototype walls. The typical behavior of the walls obtained from static analyses is discussed below. Dynamic analyses of the walls are described later.

States of Behavior Under Lateral Load

The behavior of an unbonded post-tensioned precast wall under combined lateral and gravity loads is explored using the base-shear-roof-drift relationship shown in Fig. 3(a). The base-shear-roof-drift relationship of a properly designed wall is governed by axial-flexural behavior (i.e., behavior under combined axial force and flexure). Shear slip behavior should not occur. The base shear, V, is equal to the sum of the lateral loads applied at the floor and roof levels, and the roof drift, Δ, is equal to the roof lateral displacement divided by the wall height. As the wall displaces, it goes through four states which are described below.

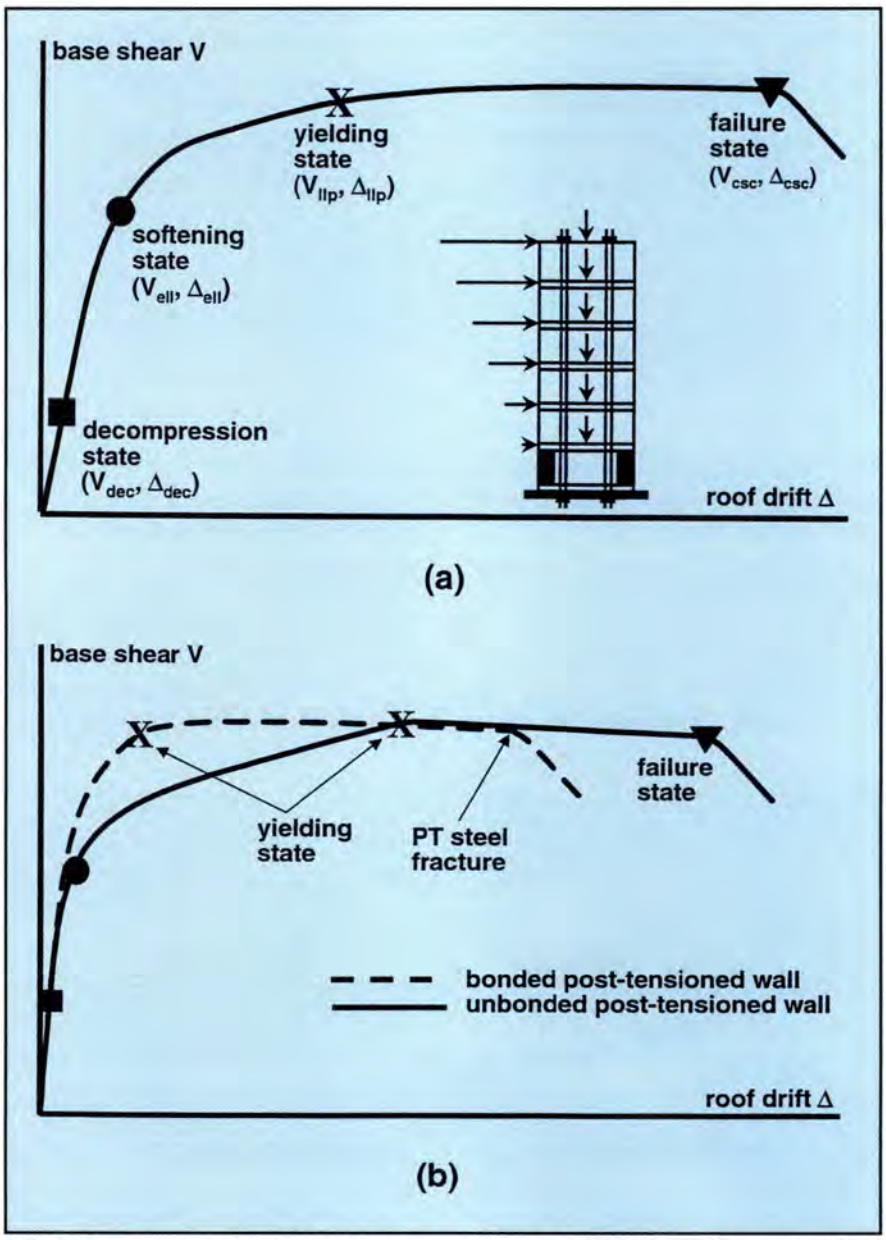

Fig. 3. Base-shear-roof-drift relationship: (a) unbonded post-tensioned precast wall; (b) effect of unbonding of the post-tensioning steel.

Decompression state — This state (indicated by a ■ marker at a base shear and roof drift of V_{dec} and Δ_{dec}, respectively) identifies the initiation of a gap opening along the horizontal joint between the wall and foundation. Gap opening initiates when the initial compression in the concrete due to the post-tensioning force and gravity load is overcome at the extreme edge at the base of the wall.

The decompression state is the beginning of nonlinear behavior of the wall due to gap opening. However, the effect of this nonlinear behavior on the lateral stiffness of the wall is small until the gap opening extends over a significant portion of the length of the horizontal joint.

Softening state — This state (indicated by a ● marker) identifies the beginning of a significant reduction in the lateral stiffness of the wall due to gap opening along the horizontal joints and nonlinear behavior of the concrete in compression. As shown in Fig. 3(a), the reduction in the lateral stiffness of the wall occurs in a smooth and continuous manner. Therefore, an effective linear limit (denoted by V_{ell} and Δ_{ell}) is used to identify the softening state.[5]

The effective linear limit may be governed by gap opening or by nonlinear behavior of the concrete depending on the stress in the concrete due to the post-tensioning force and the gravity load. If the stress in the concrete is small, the effective linear limit is governed by gap opening. If the stress in the concrete is large, the effective linear limit is governed by nonlinear behavior of the concrete.

Yielding state — This state (indicated by a **X** marker) identifies the point at which the strain in the post-tensioning steel first reaches the limit of proportionality. A properly designed wall does not reach the yielding state (denoted by V_{llp} and Δ_{llp}) until a large nonlinear drift has occurred. The nonlinearity results primarily from gap opening along the horizontal joints and nonlinear behavior of the concrete in compression. Up to the yielding state, noticeable damage to the concrete other than spalling of the cover concrete over a small region near the base of the wall is small because the spiral reinforcement provides heavy confinement.

Failure state — This state (indicated by a ▼ marker) identifies axial-flexural failure of the wall which occurs as a result of crushing of the spiral confined concrete (at V_{csc} and Δ_{csc}). Crushing of the spiral confined concrete occurs when the spiral reinforcement fractures. Sufficient spiral reinforcement is provided in the wall panels such that the failure state is reached at a drift significantly larger than the drift at the yielding state.

Effect of Unbonded Post-Tensioning

Fig. 3(b) compares the base-shear-roof-drift behavior of an unbonded post-tensioned wall and a bonded post-tensioned wall. Unbonded post-tensioned construction has the following advantages: (1) yielding of the post-tensioning steel is delayed because the strain in the post-tensioning steel is uniform over the unbonded length; (2) the post-tensioning steel does not transfer significant tensile stresses into the concrete, thus, damage in the wall panels due to cracking is reduced; (3) gap opening along the horizontal joints, primarily at the base of the wall, results in a decrease in the lateral stiffness of the wall (i.e., provides nonlinear behavior) and, thus, period elongation, with little damage to the wall; and (4) fracture of the post-tensioning steel is less likely, and thus, less critical. The effect of unbonded post-tensioning on the behavior of the wall under cyclic lateral load is described below.

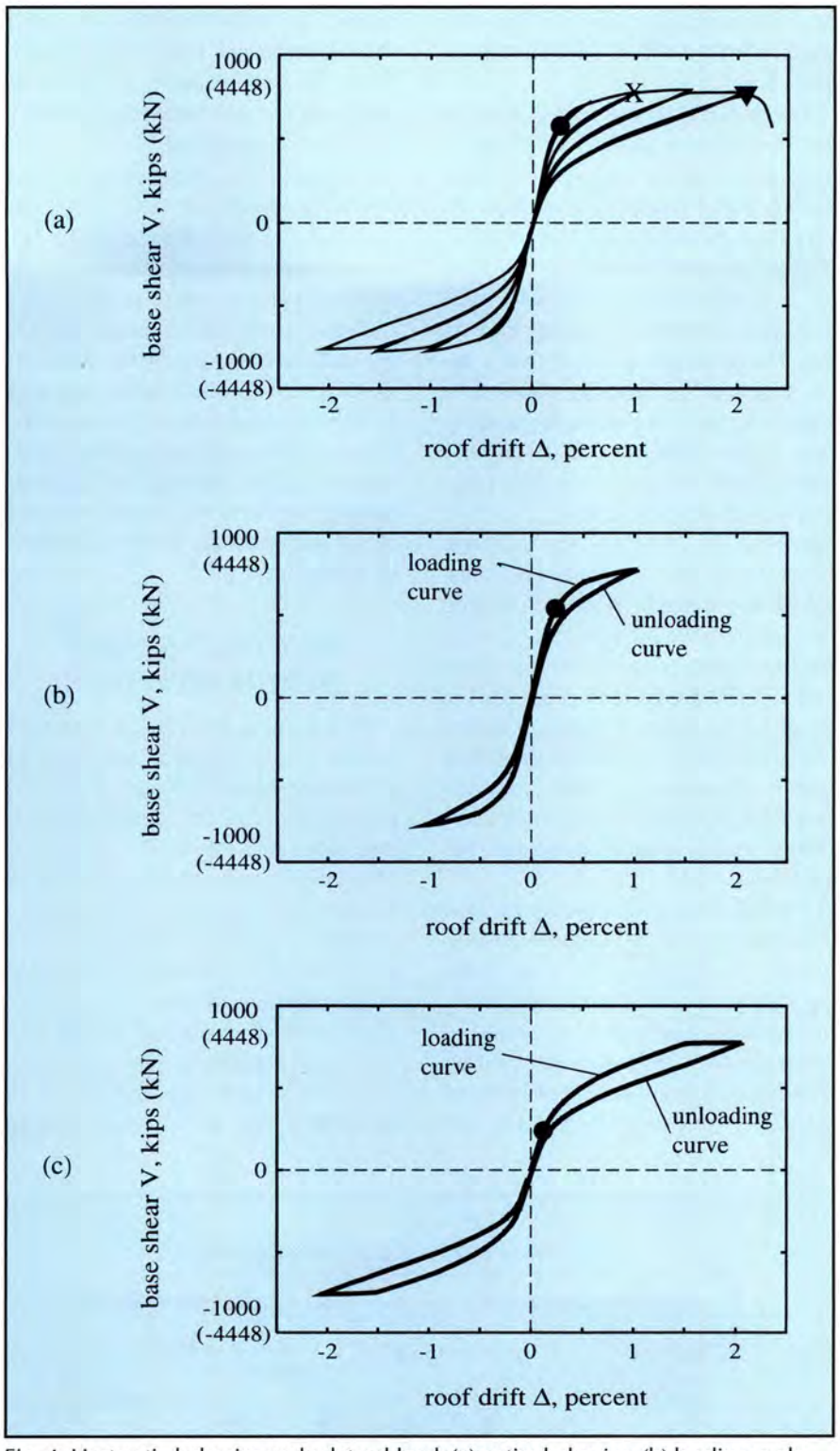

Fig. 4. Hysteretic behavior under lateral load: (a) entire behavior; (b) loading cycle just reaching the yielding state; (c) loading cycle beyond the yielding state.

Behavior Under Cyclic Lateral Load

Fig. 4 shows the base-shear-roof-drift behavior of the wall shown in Fig. 3(a) under cyclic lateral load combined with constant gravity load. The softening, yielding, and failure states under monotonic lateral load are indicated in Fig. 4(a) using the ●, **X**, and ▼ markers, respectively. Fig. 4(b) shows the behavior of the wall during a loading cycle to approximately 1 percent roof drift, just reaching the yielding state. Fig. 4(c) shows the behavior of the wall during a subsequent loading cycle to approximately 2 per-

cent roof drift, after the yielding state is exceeded but before the failure state is reached.

The hysteresis loops in Fig. 4 show that the behavior of the wall is nearly nonlinear-elastic, characterized by loading and unloading curves that are very close to each other. The behavior is close to nonlinear-elastic because the nonlinear drift occurs with little damage to the wall as discussed earlier. The nonlinear-elastic behavior results in a self-centering capability which means that upon unloading from a large nonlinear drift, the wall returns back towards its original position with little residual drift.

In Figs. 4(b) and 4(c), the softening states during the two hysteresis loops are shown using the ● marker. Before the yielding state is exceeded, V_{ell} (i.e., the base shear at the softening state) under cyclic lateral load [Fig. 4(b)] is equal to V_{ell} under monotonic lateral load [Fig. 4(a)]. After the yielding state is exceeded, V_{ell} under cyclic lateral load [Fig. 4(c)] is significantly smaller than V_{ell} under monotonic lateral load.

The reduction in V_{ell} occurs because inelastic straining of the post-tensioning steel (which occurs after the yielding state is exceeded during the previous cycles) results in a reduction in prestress. Thus, the wall softens earlier due to gap opening along the horizontal joints. Because the steel is unbonded, the inelastic strains are small even after large roof drift cycles. Thus, the reduction in prestress is small and the self-centering capability of the wall is preserved.

Unbonded post-tensioning has the following advantages under cyclic lateral load: (1) the nonlinear-elastic behavior results in a self-centering capability; (2) the decrease in the initial stiffness of the wall is small; and (3) the inelastic straining of the post-tensioning steel can be limited, and thus the reduction in prestress which results from loading cycles beyond the yielding state can be controlled. As a disadvantage, the nonlinear elastic behavior of the wall produces very little inelastic energy dissipation.

PROPOSED SEISMIC DESIGN APPROACH

This section describes a proposed seismic design approach for buildings which use unbonded post-tensioned precast walls as the primary lateral load resisting system. The plan view of a typical six-story office building in a region with high seismicity is shown in Fig. 5. The lateral load resistance of the building is provided by unbonded post-tensioned precast walls in the north-south direction and lateral load resisting frames in the east-west direction. The gravity load resistance is provided by the gravity load resisting frames, the walls, and the lateral load resisting frames. The focus in this paper is on the seismic behavior and design of the walls. Seismic behavior and design of unbonded post-tensioned precast frames is discussed by El-Sheikh et al.[8]

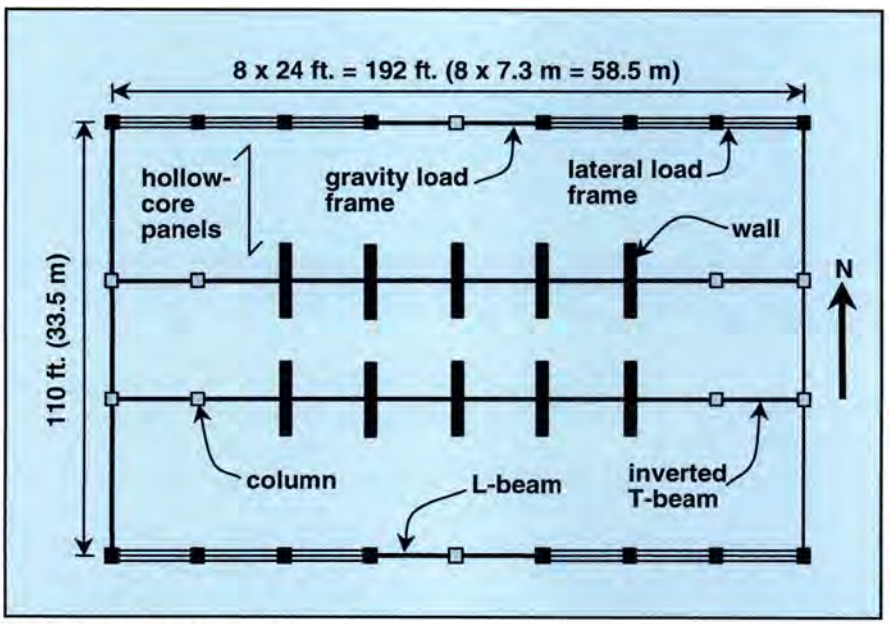

Fig. 5. Typical prototype structure.

The proposed seismic design approach is a performance-based design approach which allows the designer to specify and predict, with reasonable accuracy, the performance (degree of damage) of a building for a specified level of ground motion intensity. This requires the identification of: (1) *seismic performance levels* to describe the expected level of damage in the building during a ground motion; (2) *building limit states and capacities* to describe and quantify the damage in various structural and non-structural elements of the building; (3) *seismic input levels* to describe selected levels of ground motion intensity for a given site; and (4) *structure demands* to quantify roof drift, story drift (i.e., lateral displacement between adjacent floors divided by story height), and base shear demands for the structure.

The design approach uses three seismic performance levels: (1) the "immediate occupancy" performance level, which describes a post-earthquake damage state in which only limited structural and non-structural damage has occurred; (2) the "life safety" performance level, which describes a post-earthquake damage state in which significant damage to the building may have occurred but some margin against either total or partial structural collapse remains; and (3) the "collapse prevention" performance level, which describes a post-earthquake damage state in which the building is on the verge of partial or total collapse.

The building limit states and capacities include limit states and capacities for the unbonded post-tensioned precast walls, the lateral load resisting frames, the gravity load resisting system, and the non-structural elements. The limit states for the walls are: (1) decompression at the base; (2) decrease in the lateral stiffness; (3) spalling of cover concrete near the base; (4) yielding of the post-tensioning steel; (5) attainment of the base moment capacity; (6) reduction in the

prestress due to inelastic straining of the post-tensioning steel; (7) crushing of the concrete confined by spirals; (8) reduction in the lateral load resistance; (9) reduction in the gravity load resistance; (10) shear slip along the horizontal joints; and (11) crushing of the concrete outside the spiral confined region, but inside the region reinforced with wire mesh. Limit States 1, 2, 4, and 7 correspond to the decompression, softening, yielding, and failure states which were described earlier.

The wall design capacities which correspond to these limit states are determined from nonlinear static pushover analyses under combined lateral and gravity loads. The distribution of the lateral loads over the height of the walls is determined from the equivalent lateral force procedure in NEHRP.[9] The gravity loads (i.e., dead and live loads) are determined from the load combinations in NEHRP.

The design approach considers two seismic input levels for a given site: (1) a design level ground motion; and (2) a survival level ground motion (i.e., a maximum intensity ground motion). The design level and survival level ground motions are defined later. The structure demands are specified in terms of demands for the walls corresponding to these levels of ground motion. For the design level ground motion, the wall demands are: (1) the design base shear demand, V_{des}, (used in design to control the axial-flexural behavior); (2) the maximum roof drift demand, Δ_{des}; and (3) the maximum story drift demand, δ_{des}. For the survival level ground motion, the wall demands are: (1) the maximum roof drift demand, Δ_{sur}; and (2) the maximum base shear demand, V_{max} (used in design to prevent shear slip behavior).

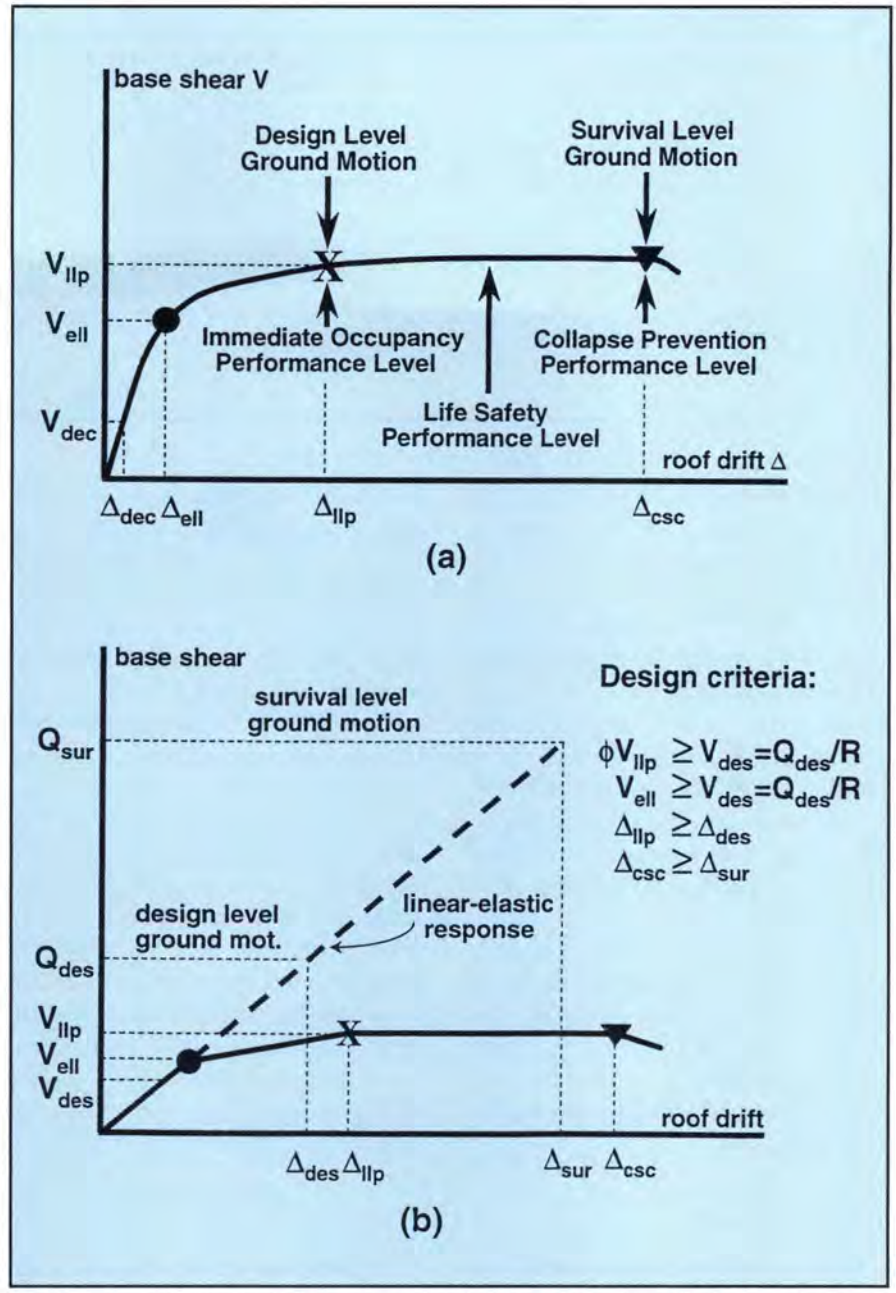

Fig. 6. Proposed seismic design approach: (a) design objectives; (b) design criteria.

Design Objectives

Design objectives relate the seismic performance levels to the seismic input levels described above as shown in Fig. 6(a). The proposed design approach has two objectives: (1) to achieve the immediate occupancy performance level under the design level ground motion; and (2) to achieve the collapse prevention performance level under the survival level ground motion.

The immediate occupancy performance level for the walls is as follows: (1) the wall behavior is nearly elastic, but nonlinear, with the nonlinear behavior being largely due to gap opening along the joints with a small contribution from nonlinear behavior of the concrete in compression; (2) the post-tensioning steel remains linear-elastic; (3) the wall panels remain nearly linear-elastic with little or no cracking, and with nonlinear behavior of concrete in compression occurring only near the bottom corners of the base panel; (4) the initial lateral load stiffness and the lateral load strength of the wall are not reduced; (5) the gravity load strength of the wall is not reduced; and (6) shear slip along the horizontal joints does not occur.

The immediate occupancy performance level for a properly designed wall is reached at the yielding state (i.e., at Δ_{llp}). Thus, Design Objective 1 can be achieved if Δ_{llp} is not exceeded under the design level ground motion [Fig. 6(a)].

The collapse prevention performance level for the walls is as follows: (1) axial-flexural compression failure of the wall does not occur; (2) the post-tensioning steel yields, however, due to unbonding, the inelastic strains are not large; (3) inelastic straining of

Table 1. Proposed seismic design approach.

Seismic input level	Seismic performance level	Design criteria
Design level ground motion	Immediate occupancy	$\phi_f V_{llp} \geq V_{des}$
		$V_{ell} \geq V_{des}$
		$\Delta_{llp} \geq \Delta_{des}$
		$\delta_{des} \leq \delta_{all}$
Survival level ground motion	Collapse prevention	$\Delta_{csc} \geq \Delta_{sur}$
		$\Delta_{ctc} \geq \Delta_{csc}$
		$\phi_s V_{ss} \geq V_{max}$
		$\Delta_{sur} \leq \Delta_g$

the post-tensioning steel results in a reduction in the prestress, however, the self-centering capability of the wall is preserved; (4) the wall softens earlier due to the reduction in prestress, however, the initial lateral load stiffness and the lateral load strength of the wall are not reduced; (5) the gravity load strength of the wall is not reduced; (6) as a result of the self-centering capability, the residual lateral drift of the wall is not excessive; and (7) shear slip along the horizontal joints does not occur.

The collapse prevention performance level for a properly designed wall is reached at the failure state (i.e., at Δ_{csc}). Thus, Design Objective 2 can be achieved if Δ_{csc} is not exceeded under the survival level ground motion [Fig. 6(a)].

Design Criteria

Seismic design criteria specify required comparisons between estimated structure design demands and structure design capacities. If the capacities exceed the demands, the design objectives are achieved. Design of an unbonded post-tensioned precast wall involves establishing wall design demands and providing wall design capacities so that all of the design criteria are satisfied. The design approach includes eight design criteria which are described below and summarized in Table 1. Procedures for estimating the design demands and capacities are not described below in full detail, however, they are given by Kurama et al.[6]

1. Criterion for the base shear capacity at the yielding state, V_{llp} — This design criterion is described using the idealized, trilinear base-shear-roof-drift relationship of a wall shown in Fig. 6(b). The trilinear relationship is determined from the softening, yielding, and failure states obtained from static push-over analysis as described above and shown in Fig. 3(a).

According to the design approach, the base shear capacity at the yielding state, V_{llp}, is required to be larger than the design base shear demand, V_{des} [Fig. 6(b)]. The design base shear demand, V_{des}, is equal to the linear-elastic base shear demand for the design level ground motion, Q_{des}, divided by a response modification coefficient, R, in accordance with the equivalent lateral force procedure in NEHRP.[9] A capacity reduction factor, ϕ_f, is applied to V_{llp} in accordance with the provisions of the ACI 318 Code.[10] Thus:

$$\phi_f V_{llp} \geq V_{des} = \frac{Q_{des}}{R} \qquad (1)$$

2. Criterion for the base shear capacity at the softening state, V_{ell} — The purpose of this criterion is to prevent a premature reduction in the lateral stiffness of the wall. The design approach requires that the base shear capacity at the softening state, V_{ell}, is larger than the design base shear demand, V_{des} [Fig. 6(b)]. A capacity reduction factor is not applied to V_{ell} because the consequences of V_{des} exceeding V_{ell} are not considered to be serious. Thus:

$$V_{ell} \geq V_{des} = \frac{Q_{des}}{R} \qquad (2)$$

3. Criterion for the roof drift capacity at the yielding state, Δ_{llp} — In order to achieve Design Objective 1, the roof drift capacity at the yielding state, Δ_{llp}, is required to be larger than the expected maximum roof drift demand under the design level ground motion, Δ_{des} (Δ_{des} can be estimated from linear-elastic analysis results using an equal displacement assumption as described later). Thus:

$$\Delta_{llp} \geq \Delta_{des} \qquad (3)$$

4. Criterion for the maximum story drift under the design level ground motion, δ_{des} — The purpose of this criterion is to control the initial stiffness of the wall and to control damage to basic access and life safety systems. The NEHRP provisions[9] specify an allowable story drift, δ_{all}. Accordingly, the expected maximum story drift demand under the design level ground motion, δ_{des}, is required to be smaller than δ_{all} (δ_{des} can be estimated from linear-elastic analysis results as described later). Thus:

$$\delta_{des} \leq \delta_{all} \qquad (4)$$

5. Criterion for the roof drift capacity at the failure state, Δ_{csc} — To achieve Design Objective 2, the roof drift capacity at the failure state, Δ_{csc}, is required to be larger than the expected maximum roof drift demand under the survival level ground motion, Δ_{sur} (Δ_{sur} can be estimated from linear-elastic analysis results as described later). Thus:

$$\Delta_{csc} \geq \Delta_{sur} \qquad (5)$$

6. Criterion for the size of the spiral confined region near the base — The purpose of this criterion is to prevent crushing of the concrete in the region reinforced only with wire mesh (Fig. 1). The length and height of the spiral confined wall region near the base should be large enough to prevent crushing of the concrete inside the wire mesh. The design approach requires that the roof drift capacity corresponding to the crushing of the concrete inside the wire mesh, Δ_{ctc}, is larger than the roof drift capacity at the failure state, Δ_{csc}. Thus:

$$\Delta_{ctc} \geq \Delta_{csc} \qquad (6)$$

7. Criterion for the shear slip capacity, V_{ss} — The purpose of this criterion is to prevent shear slip along the horizontal joints. The most critical joint for shear slip is the base-panel-to-foundation joint because the shear demand is maximum at the base while the shear slip capacity is nearly uni-

form over the wall height due to the post-tensioning.[6] The design approach requires that the expected minimum shear slip capacity at the base, V_{ss}, is larger than the expected maximum base shear demand under the survival level ground motion, V_{max} (the estimation of V_{ss} and V_{max} is described later). A capacity reduction factor, ϕ_s, is applied to V_{ss} in accordance with the ACI 318 Code.[10] Thus:

$$\phi_s V_{ss} \geq V_{max} \quad (7)$$

8. Criterion for the maximum roof drift under the survival level ground motion, Δ_{sur} — The purpose of this criterion is to prevent premature failure of the gravity load resisting system which is not part of a lateral load resisting system, due to excessive drift. Design of the gravity load system is not addressed in this paper. However, it is assumed that the gravity load system can be designed to sustain a roof drift of $\Delta_g = 2.5$ percent. The design approach requires that the expected maximum roof drift demand under the survival level ground motion, Δ_{sur} is smaller than Δ_g. Thus:

$$\Delta_{sur} \leq \Delta_g = 2.5 \text{ percent} \quad (8)$$

PROPOSED SEISMIC DESIGN PROCEDURE

This section describes the proposed seismic design procedure for unbonded post-tensioned precast walls. This procedure is based on a parametric investigation which was conducted to determine how the wall design capacities V_{llp}, V_{ell}, Δ_{llp}, and Δ_{csc} are affected by changes in wall design properties. The wall design properties that were considered include: (1) initial stress in the post-tensioning steel, f_{pi}; (2) total area of the post-tensioning steel, A_p; (3) wall length, l_w; (4) location of the post-tensioning steel; (5) unbonded length of the post-tensioning steel, l_{unb}; (6) wall panel spiral reinforcement ratio, ρ_{sp}; (7) amount of gravity load, G; (8) unconfined concrete compressive strength, f_c'; and (9) wall thickness, t_w.

Approximately 200 nonlinear static push-over analyses of a number of walls which differ in only one or two of the design properties were conducted. The properties of the walls which were used in this parametric investigation are described in detail by Kurama et al.[5] The design capacities of the walls were determined from the base-shear-roof-drift relationships obtained from the analyses. Figs. 7(a) through 7(g) show the base-shear-roof-drift relationships of some of the walls. The base shear resistance of the walls is normalized by V_{llp} of a selected wall[5] with a particular set of properties, for which V_{llp} = 358 kips (1592 kN) [see Fig. 7(e)].

The results in Fig. 7 suggest relationships between the wall design properties and the wall design capacities. For example, Figs. 7(a) and 7(b) show that V_{ell} is significantly affected by f_{pi} and A_p.

Fig. 7(c) shows the normalized base-shear-roof-drift relationship of four walls where both f_{pi} and A_p are varied such that the total post-tensioning force, P_i, remains constant ($P_i = A_p f_{pi}$). This figure shows that V_{ell} remains constant when P_i remains constant. Thus, after selecting trial wall dimensions (i.e., wall length, l_w and wall thickness, t_w), the first step toward a design that satisfies the design criteria is to set f_{pi} to a desired value (usually 55 to 65 percent of the ultimate strength of the post-tensioning steel, f_{pu}). Then, A_p is determined such that $V_{ell} \leq V_{des}$ to satisfy Design Criterion 2.

Figs. 7(b) and 7(d) show that V_{llp} is significantly affected by A_p and l_w. Thus, the next step in design is to check that A_p and l_w are large enough so that $\phi_f V_{llp} \geq V_{des}$ to satisfy Design Criterion 1.

The next step in design is to check that $\delta_{des} \leq 1.5$ percent and $\Delta_{sur} \leq 2.5$ percent to satisfy Design Criteria 4 and 8, respectively. Deflections δ_{des} and Δ_{sur} are estimated from the linear-elastic lateral stiffness of the wall estimated using the wall length, l_w, and the wall thickness, t_w.

Figs. 7(a), 7(e), and 7(f) show that Δ_{llp} is significantly affected by f_{pi}, l_{unb}, and the location of the post-tensioning steel. Typically, l_{unb} is equal to the wall height to take full advantage of unbonded construction. Thus, the next step in design is to check that f_{pi} and the location of the post-tensioning steel are such that $\Delta_{llp} \geq \Delta_{des}$ to satisfy Design Criterion 3. It is recommended that the post-tensioning steel is located between the two regions of spiral confined concrete so that the spiral confined regions are not weakened by the presence of the post-tensioning ducts.

The next step in design is to check that $\phi_s V_{ss} \leq V_{max}$ to satisfy Design Criterion 7. This is discussed in more detail later.

Fig. 7(g) shows that Δ_{csc} is significantly affected by the amount of spiral reinforcement, ρ_{sp}. Thus, the final step in design is to provide sufficient spiral reinforcement so that $\Delta_{csc} \geq \Delta_{sur}$ to satisfy Design Criterion 5. Based on the nonlinear static and nonlinear dynamic analyses conducted in this research, it is recommended that interlocking spiral reinforcement is provided over a length equal to, at least, one-quarter of the wall length near each bottom corner and over a height greater than or equal to the first story, so that $\Delta_{ctc} \geq \Delta_{csc}$ to satisfy Design Criterion 6.

DESIGN OF PROTOTYPE WALLS

Six six-story prototype walls were designed using the design approach and the design procedure described above. The prototype walls were designed for sites in two different seismic regions (regions with high seismicity and regions with moderate seismicity) and for sites with three different soil characteristics (stiff soil, medium soil, and soft soil characteristics). The prototype walls were designed using the 1991 edition of the NEHRP provisions[9] as described below. This edition of the NEHRP provisions was used because the prototype walls were designed before the 1994 edition was published in May 1995.

The design level and survival level ground motions which were used in the design of the prototype walls were determined from the 1991 edition of the NEHRP provisions. The design level ground motion is the NEHRP design ground motion and has a 90 percent probability of not being exceeded in 50 years, corresponding approximately to a 500-year return period. The prototype walls were designed for a design level ground motion with a peak acceleration of 0.40g and 0.10g

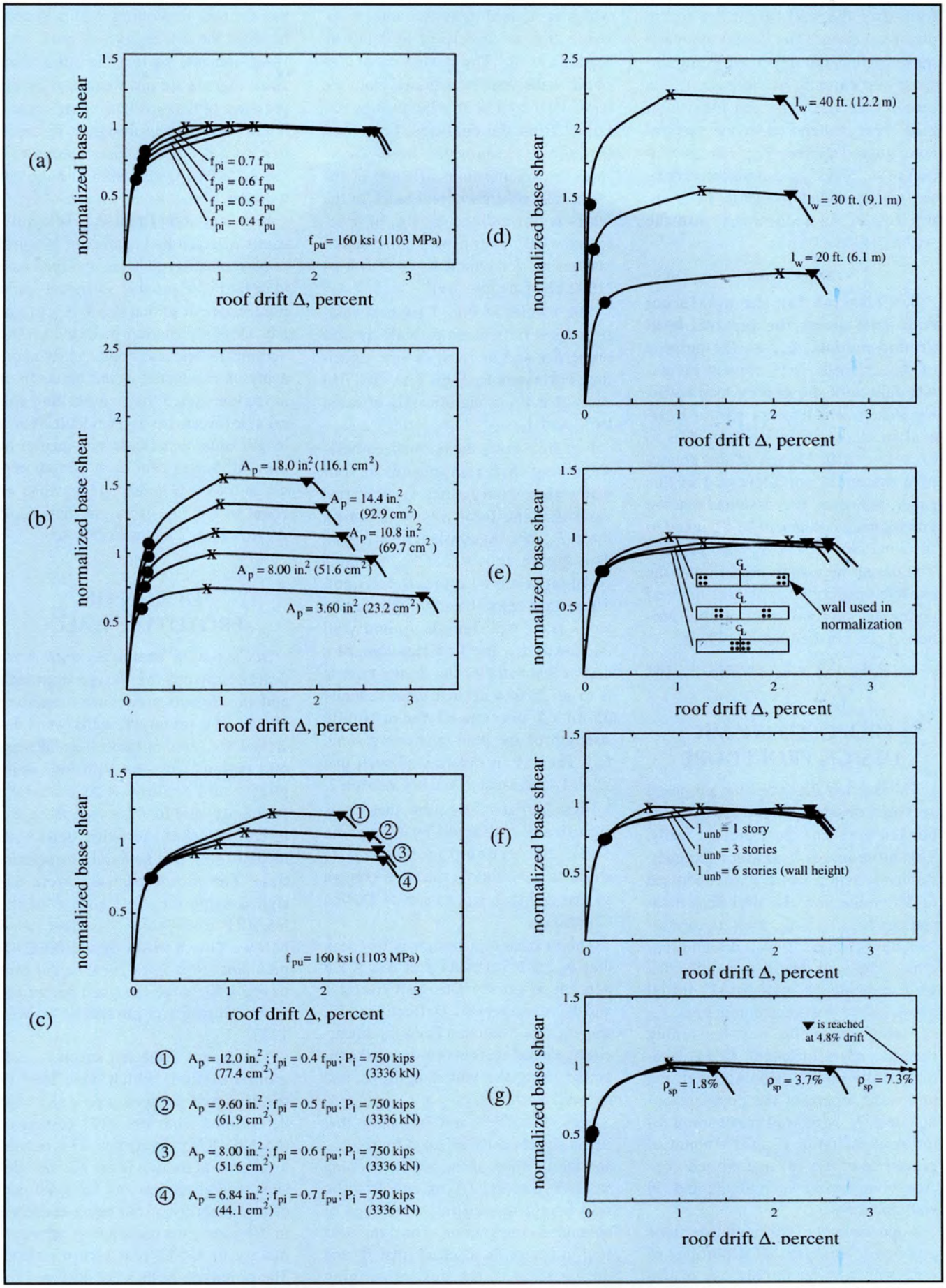

Fig. 7. Effect of wall structural properties on wall design capacities: (a) initial steel stress, f_{pi}; (b) total steel area, A_p; (c) f_{pi} and A_p; (d) wall length, l_w; (e) steel location; (f) unbonded length, l_{unb}; (g) spiral ratio, ρ_{sp}.

in regions of high seismicity and moderate seismicity, respectively.

The survival level ground motion has approximately a 90 percent probability of not being exceeded in 250 years. The prototype walls were designed for a survival level ground motion with a peak acceleration of $1.0g$ and $0.25g$ in regions of high seismicity and moderate seismicity, respectively. Quantification of these ground motions is described by Kurama et al.[6]

In the design of the prototype walls, $R = 4.5$ was used in Design Criteria 1 and 2, and $\delta_{all} = 1.5$ percent was used in Design Criterion 4 as specified by the 1991 edition of the NEHRP provisions.[9] Capacity reduction factors of $\phi_f = 0.75$ (for axial compression and flexure) and $\phi_s = 0.85$ (for shear) were used in Design Criteria 1 and 7, respectively, in accordance with the ACI 318 Code.[10]

Additional work is needed to investigate the effects of the differences between the 1991 edition of the NEHRP provisions and the current 1997 edition on the seismic design and dynamic response evaluation of the prototype walls. There are differences in the design level ground motion, in the coefficients related to the site soil characteristics, and in the R and δ_{all} values specified by the two editions.

In the 1991 edition, $R = 4.5$ is specified for reinforced concrete bearing wall systems and $\delta_{all} = 1.5$ percent is specified for buildings with more than

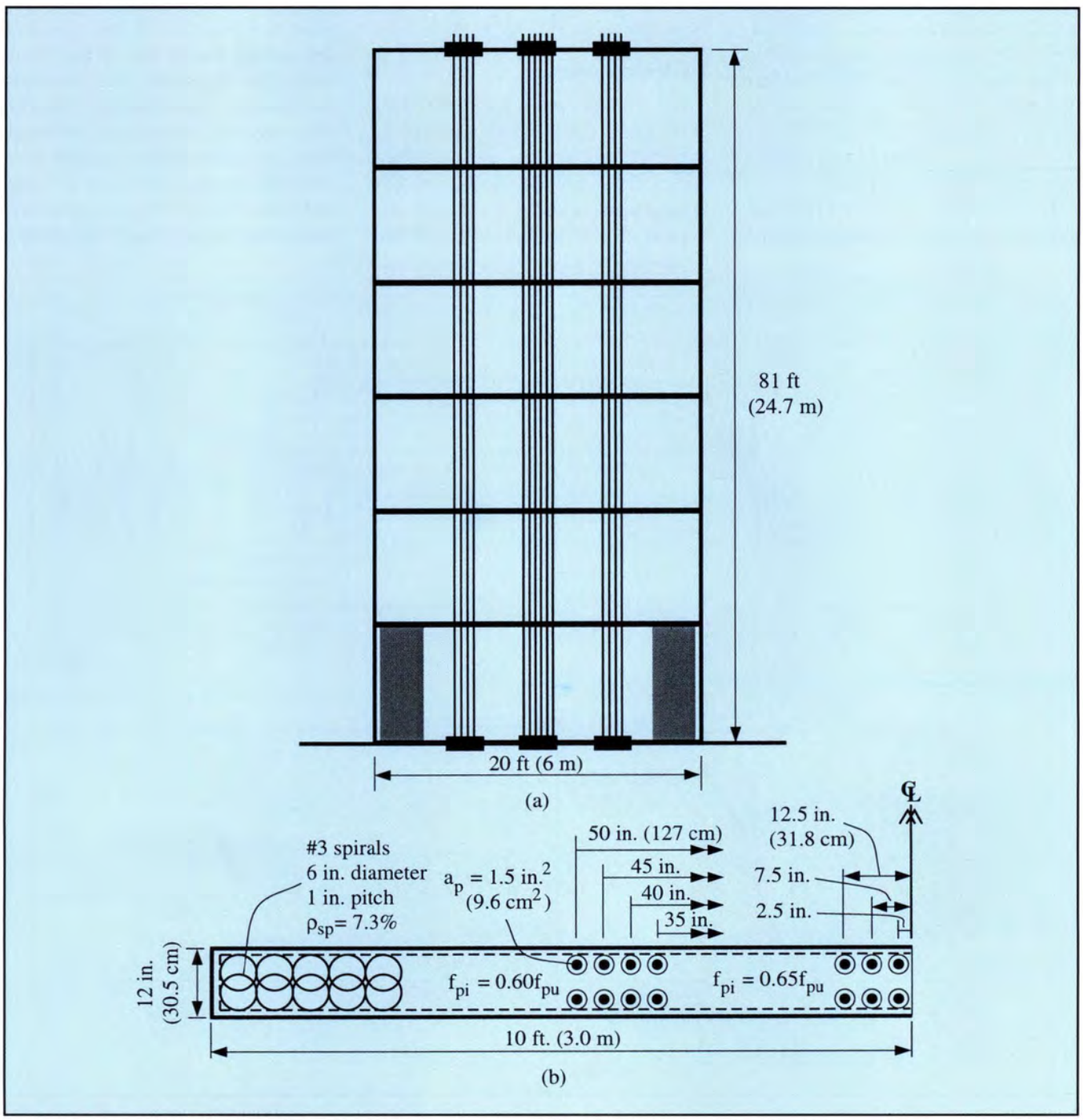

Fig. 8. Properties of Wall WH1: (a) elevation; (b) cross section near base (enlarged).

four stories. In the 1997 edition, R = 5.5 is specified for special reinforced concrete bearing walls and δ_{all} = 2.0 percent is specified for buildings with more than four stories. There are additional differences in the combination of earthquake loads and gravity loads in the two editions.

BEHAVIOR OF PROTOTYPE WALLS UNDER EARTHQUAKE LOAD

This section describes the expected dynamic response of the prototype walls under earthquakes. The prototype walls were designed as described above, and more than 200 nonlinear dynamic time-history analyses of these walls were conducted using a total of 15 design level and 15 survival level ground motion records.[6]

The following sections focus on the dynamic analyses of the prototype walls designed for regions with high seismicity. The dynamic analyses of the prototype walls that were designed for regions with moderate seismicity are discussed by Kurama et al.[6] Fig. 8 shows the properties of one of the prototype walls (referred to as Wall WH1) designed for a region with high seismicity and a site with a medium soil profile, for the prototype structure shown in Fig. 5. Most of the discussion in this section is based on this wall. The dynamic analyses were conducted with a viscous damping ratio of 3 percent and a time step of 0.01 seconds.

Hysteretic Behavior

Fig. 9 shows the response of Wall WH1 under the Hollister ground motion (recorded on a site with a medium soil profile during the 1989 Loma Prieta earthquake) scaled to a peak acceleration of 1.0g to represent a severe survival level ground motion. This ground motion was selected from a larger set of ground motions and has the potential to severely damage Wall WH1.[6] The behavior of Wall WH1 under static cyclic lateral load was shown previously in Fig. 4.

Fig. 9(a) shows the base-moment-base-rotation hysteretic response and the heavy solid line in Fig. 9(b) shows the roof-drift time-history. Figs. 9(c) and 9(d) show two hysteresis loops taken from Fig. 9(a). Fig. 9(c) shows a hysteresis loop before the yielding state is reached [between 6.3 and 7.5 seconds as indicated by two solid dots and vertical dashed lines in Fig. 9(b)], before the large roof drift excursion that occurs at approximately 8 seconds. Similarly, Fig. 9(d) shows a hysteresis loop after the yielding state has been exceeded [between 26.1 and 27.7 seconds, also indicated by two solid dots and vertical dashed lines in Fig. 9(b)].

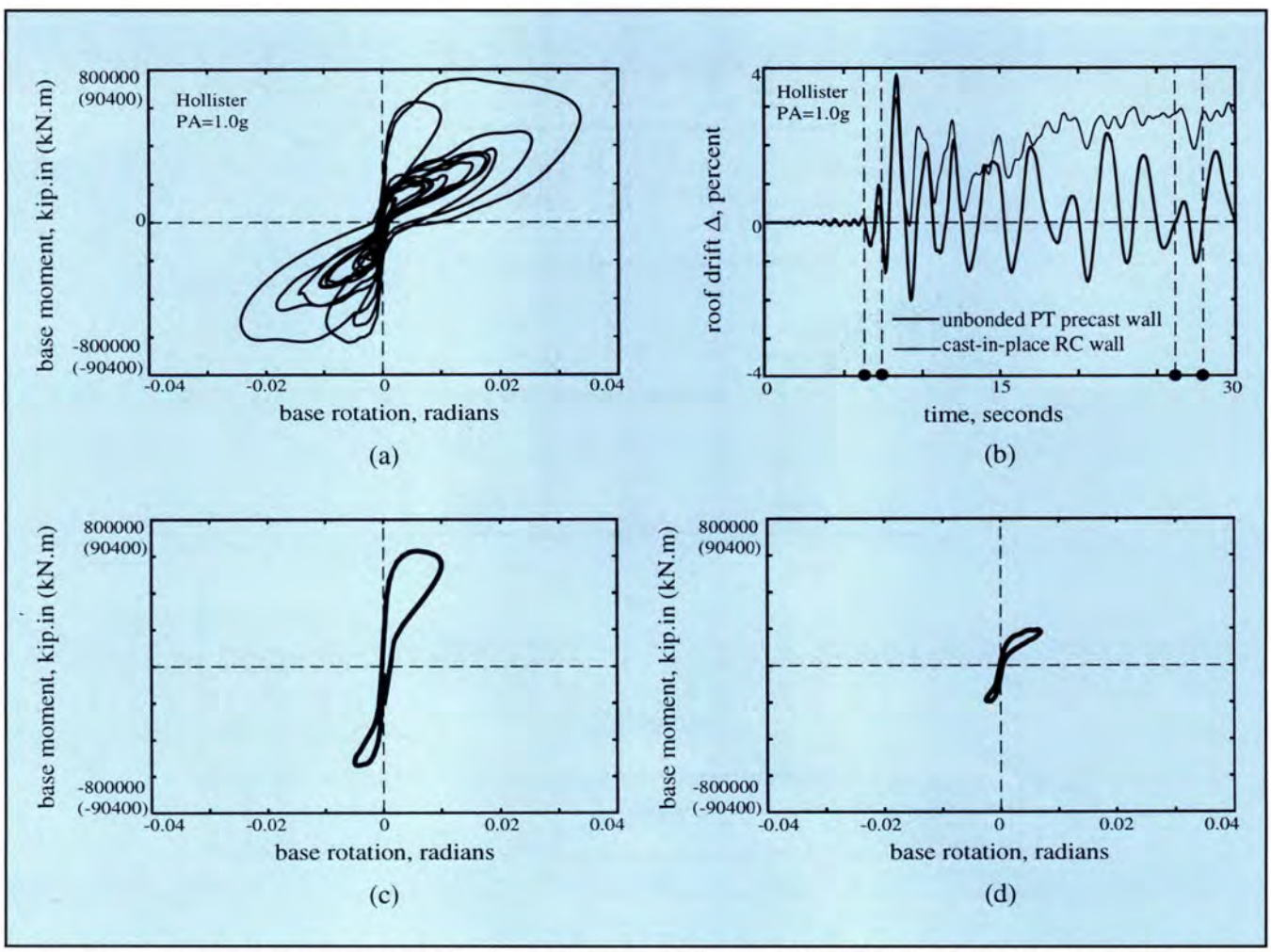

Fig. 9. Behavior under earthquake load: (a) base-moment-base-rotation hysteresis; (b) roof-drift time-history; (c) response between time = 6.3 and 7.5 seconds; (d) response between time = 26.1 and 27.7 seconds.

The shape of the hysteresis loops under dynamic loading (Fig. 9) are similar to those under static cyclic loading (Fig. 4). The hysteresis loop in Fig. 9(c) dissipates more energy than the hysteresis loop in Fig. 4(b) because of the 3 percent viscous damping that was used in the dynamic analysis.

Figs. 9(c) and 9(d) show that softening of the wall occurs at a smaller base moment after the yielding state has been exceeded in a previous cycle (as discussed earlier using Fig. 4). Because of the early softening, the maximum base moment reached during the hysteresis loop in Fig. 9(d) is smaller than the maximum base moment reached during the hysteresis loop in Fig. 9(c) (even though the roof drifts reached during the two loops are similar). It is noted that the reduction in the maximum base moment reached in Fig. 9(d) indicates a reduction in the moment at which the wall softens, and not a reduction in the ultimate strength of the wall. As shown in Fig. 4(c), there is no significant reduction in the ultimate strength of the wall until the failure state is exceeded.

Fig. 9(b) shows a comparison between the roof-drift time-history of Wall WH1 (heavy solid line) and the roof-drift time-history of a cast-in-place reinforced concrete wall (light solid line). The cast-in-place wall has the same strength, initial stiffness, drift capacity, initial fundamental period, and viscous damping as Wall WH1. Thus, the only difference between the walls is their hysteretic behavior under lateral load. The hysteretic behavior of Wall WH1 is shown in Fig. 4. The inelastic energy dissipation of the cast-in-place wall is approximately twice the inelastic energy dissipation of Wall WH1. However, the cast-in-place wall does not have a self-centering capability.[6]

Three important differences are observed between the response of Wall WH1 and the cast-in-place wall: (1) the maximum roof drift of Wall WH1 is larger than that of the cast-in-place wall; (2) the response of Wall WH1 decays (damps out) less rapidly resulting in a large number of large drift cycles; and (3) Wall WH1 oscillates around the zero-drift position, whereas, the cast-in-place wall accumulates a significant residual drift (residual roof drift ≈ 3 percent).

Based on the results of the dynamic analyses (using seven ground motions recorded on sites with a medium soil profile), the maximum roof drift of Wall WH1 is, on average, 38 percent larger than that of the cast-in-place wall under design level ($0.40g$) ground motions, and 41 percent larger than that of the cast-in-place wall under survival level ($1.0g$) ground motions.[6]

Maximum Roof Drift and Story Drift Demands

Satisfactory seismic response of an unbonded post-tensioned precast wall depends on the maximum roof drift reached during a ground motion. For a design level ground motion, if the maximum roof drift exceeds the expected maximum roof drift demand, Δ_{des}, or if the maximum story drift exceeds the expected maximum story drift demand, δ_{des}, unexpected structural and/or nonstructural damage may occur. For a survival level ground motion, if the maximum roof drift exceeds the expected maximum roof drift demand, Δ_{sur}, the wall may suffer an axial-flexural compression failure due to crushing of the spiral confined concrete. Thus, accurate estimates of Δ_{des}, δ_{des}, and Δ_{sur} are needed for design.

In the design of the prototype walls, Δ_{des}, δ_{des}, and Δ_{sur} were estimated using an equal displacement assumption. According to the equal displacement assumption, a nonlinear system and a linear-elastic system with the same initial fundamental (first mode) period have similar maximum drift demands for a given ground motion. Thus, Δ_{des}, δ_{des}, and Δ_{sur} are estimated from linear-elastic analysis results [Fig. 6(b)].

For the linear-elastic analysis, the distribution of the lateral forces over the height of the wall is determined using the equivalent lateral force procedure in NEHRP.[9] The gravity loads (i.e., dead and live loads) are determined from the load combinations in NEHRP. The deflections Δ_{des} and δ_{des} are the roof drift and the maximum story drift (which occurs in the top story) at a base shear equal to the linear-elastic base shear demand for the design level ground motion, Q_{des} [Fig. 6(b)]. Δ_{sur} is the roof drift at a base shear equal to the linear-elastic base shear demand for the survival level ground motion, Q_{sur}. Q_{des} and Q_{sur} are calculated using the NEHRP design response spectrum[9] scaled to represent either the design level or the survival level ground motion.

The equal displacement assumption is usually applicable to structural systems with wide and stable (i.e., ductile) hysteresis loops, with fundamental periods longer than, approximately, 0.5 seconds, and located on sites with a stiff soil profile.[11] The prototype walls have fundamental periods which are longer than 0.5 seconds and have stable but narrow hysteresis loops. The applicability of the equal displacement assumption to the prototype walls is discussed below using Fig. 10.

Figs. 10(a) and (b) show the roof-drift time-history of Wall WH1 under the Newhall ground motion (recorded on a site with a medium soil profile during the 1994 Northridge earthquake) scaled to peak accelerations of $0.40g$ and $1.0g$ to represent design level and survival level ground motions, respectively. Similarly, Figs. 10(c) and (d) show the roof-drift time-history of another prototype wall, Wall WH4, designed for a region with high seismicity and a site with a soft soil profile, under the Foster City ground motion (recorded on a site with a soft soil profile during the 1989 Loma Prieta earthquake) scaled to $0.40g$ and $1.0g$. Similar to the Hollister ground motion, the Newhall and Foster City ground motions were selected from a larger set of ground motions and have the potential to severely damage Walls WH1 and WH4.[6] Walls WH1 and WH4 have fundamental periods of 0.65 and 0.50 seconds, respectively.

Fig. 10 shows that the Δ_{des} and Δ_{sur} values estimated using the equal displacement assumption (indicated by the dashed horizontal lines) underestimate the maximum roof drift reached during the dynamic analyses.

The maximum roof drift demand for Wall WH1 estimated using the equal displacement assumption is Δ_{des} = 0.81 percent and Δ_{sur} = 2.0 percent for

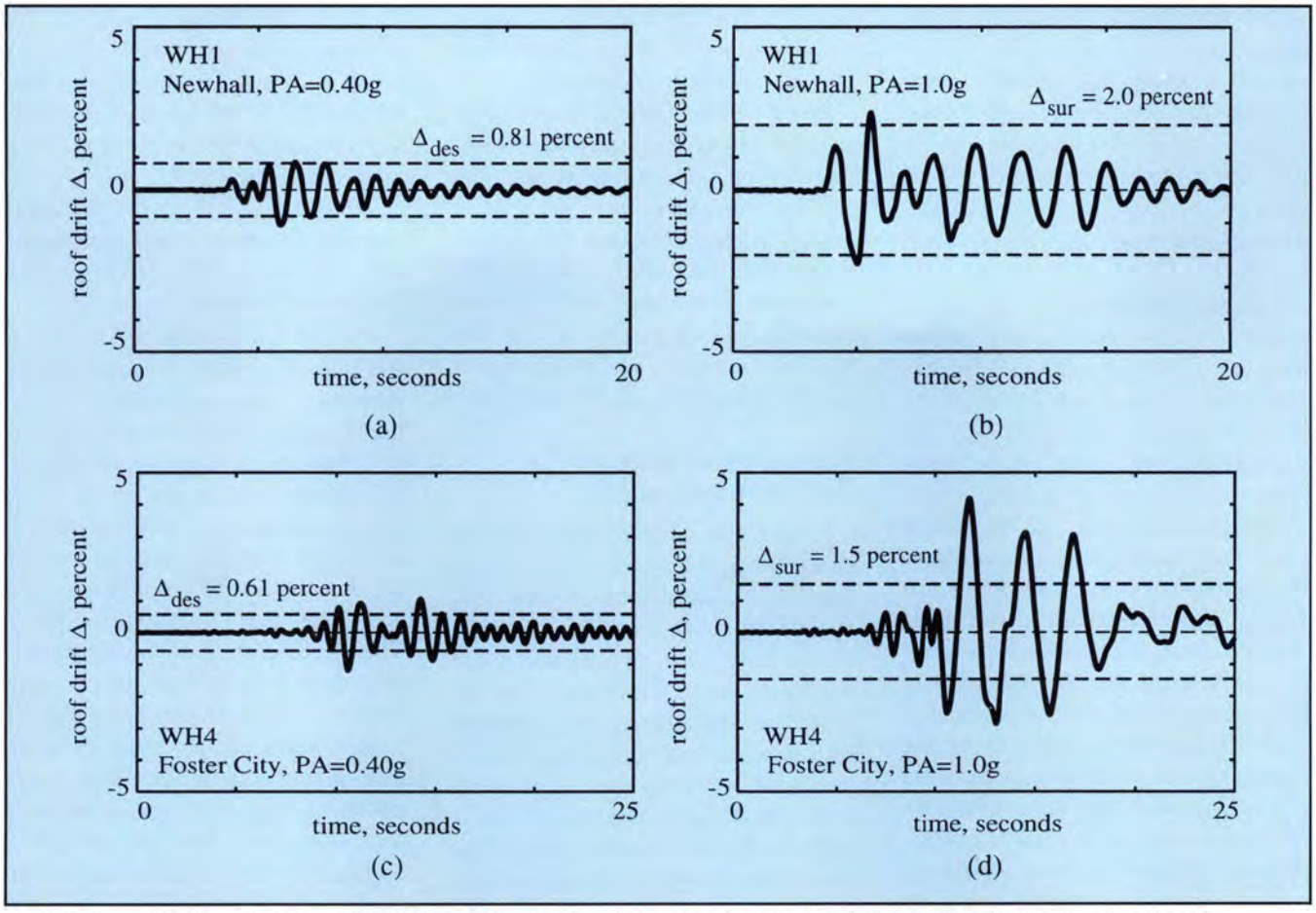

Fig. 10. Roof-drift time-history: (a) Wall WH1 under the Newhall ground motion scaled to 0.40*g*; (b) Wall WH1 under the Newhall ground motion scaled to 1.0*g*; (c) Wall WH4 under the Foster City ground motion scaled to 0.40*g*; (d) Wall WH4 under the Foster City ground motion scaled to 1.0*g*.

the design level and survival level ground motions, respectively. The average maximum roof drift obtained from the dynamic analyses (using seven ground motions recorded on sites with a medium soil profile) is 0.93 percent and 3.2 percent for the design level (0.40*g*) and survival level (1.0*g*) ground motions, respectively.[6]

Similarly for Wall WH4, the maximum roof drift demand estimated using the equal displacement assumption is Δ_{des} = 0.61 percent and Δ_{sur} = 1.5 percent for the design level and survival level ground motions, respectively. The average maximum roof drift obtained from the dynamic analyses (using three ground motions recorded on sites with a soft soil profile) is 0.91 and 3.9 percent for the design level (0.40*g*) and survival level (1.0*g*) ground motions, respectively.[6]

The difference between the estimated maximum roof drift demand and the maximum roof drift from the dynamic analyses is larger for the survival level ground motions than for the design level ground motions, and is larger for walls designed for sites with a soft soil profile than for sites with a medium soil profile. The results also indicate that there is a large scatter in the maximum roof drift demand for sites with medium or soft soil profiles, particularly for the survival level ground motions.

The dynamic analysis results show that the equal displacement assumption would, on average, provide a reasonable estimate of the maximum roof drift demands for walls designed for sites with a stiff soil profile but not for sites with medium or soft soil profiles. Improved methods to estimate the maximum roof drift demands for walls designed for sites with medium or soft soil profiles are needed for design.

Post-Tensioning Steel Forces

This section investigates the reduction in prestress that occurs due to inelastic straining of the post-tensioning steel during loading cycles beyond the yielding state as described earlier. Fig. 11(a) shows the time-history of the total force in the post-tensioning steel in Wall WH1 during the Newhall ground motion scaled to peak accelerations of 0.40*g* and 1.0*g* representing design level and survival level ground motions, respectively. The total post-tensioning steel force is normalized with respect to the total ultimate strength of the post-tensioning steel.

Fig. 11(a) shows that there is a significant reduction in the total post-tensioning steel force under the survival level (1.0*g*) ground motion. This is explained below using Fig. 11(b), which shows the roof-drift time-histories of the wall during the two ground motions [which are also shown in Figs. 10(a) and 10(b)]. The horizontal lines in Fig. 11(b) indicate the roof drift at which the yielding state is reached (i.e., Δ_{llp} = 0.82 percent) during static push-over analysis of the wall.

The local maxima on the post-tensioning steel force time-histories in Fig. 11(a) correspond to local maxima in the roof-drift time-histories in Fig. 11(b) (i.e., maximum total post-tensioning steel forces are reached at maximum roof drift). The local minima on the post-tensioning steel force time-histories correspond to times of zero roof drift. The reduction in the total post-tensioning steel force at zero roof drift which occurs in Fig. 11(a) is a measure of the reduction in prestress due to inelastic straining of the post-tensioning steel.

During the design level ($0.40g$) ground motion, the maximum inelastic strain reached in the post-tensioning steel is very small and, thus, the corresponding reduction in prestress is very small. As shown in Fig. 11(a), there is a very small reduction in prestress at around 6 seconds which occurs as a result of the inelastic straining of the post-tensioning steel when the roof drift at the yielding state (Δ_{llp}) is exceeded as shown in Fig. 11(b).

During the survival level ($1.0g$) ground motion, significant yielding of the post-tensioning steel occurs, resulting in a significant reduction in prestress. The solid line in Fig. 11(b) shows a large positive roof drift cycle around 4 seconds which significantly exceeds Δ_{llp}. This results in inelastic straining of the post-tensioning steel and reduction of the total post-tensioning steel force at zero roof drift as shown in Fig. 11(a), thus, a reduction in prestress occurs. In the two subsequent roof drift cycles, Δ_{llp} is exceeded even further, resulting in additional inelastic straining of the post-tensioning steel, and thus, additional reduction in prestress. The roof drift cycles that follow are smaller and do not cause further reduction in prestress.

As described earlier, the proposed design approach requires that Δ_{llp} is not reached under the design level ground motion [Fig. 6(a)]. Thus, reduction in prestress under the design level ground motion should not occur. Under the survival level ground motion, roof drift cycles that significantly exceed Δ_{llp} are allowed by the design approach, possibly resulting in significant reduction in prestress as shown in Fig. 11(a).

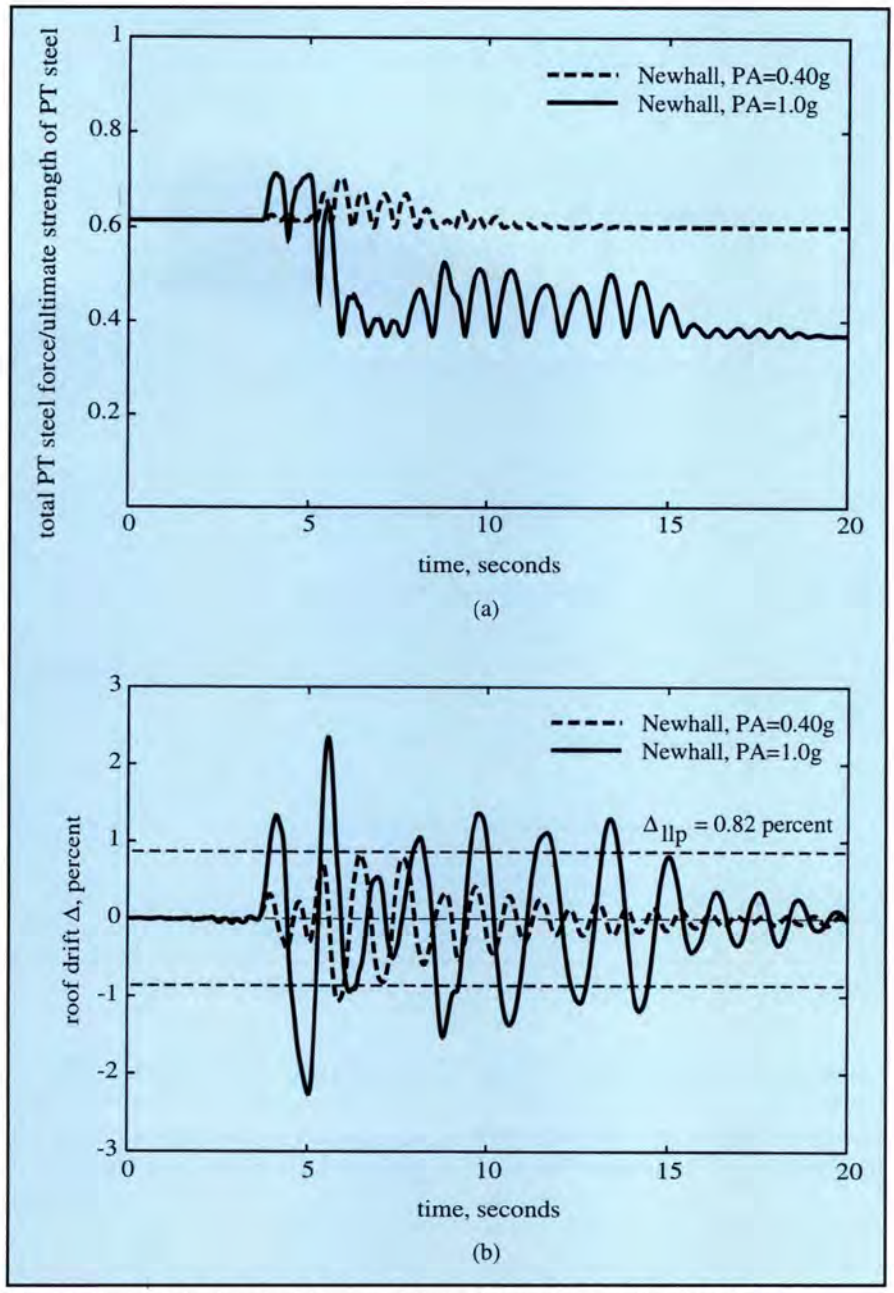

Fig. 11. Post-tensioning steel forces: (a) time-history of normalized total post-tensioning (PT) steel force; (b) time-history of roof drift.

The reduction in prestress has two important effects on the dynamic response: (1) it changes the hysteretic behavior of the wall as shown in Fig. 9(a) and described using Fig. 4 (i.e., earlier softening of the wall occurs, however, the self-centering capability is preserved); and (2) it significantly reduces the shear slip capacity of the wall as discussed in the next section. It is important that the reduction in prestress is considered in the seismic design of walls for the survival level ground motion. The proposed design approach includes a method to estimate the maximum reduction in prestress under the survival level ground motion, which can be found in Kurama et al.[6]

Shear Slip

As described earlier, the proposed design approach requires that shear slip along the horizontal joints is prevented (i.e., $\phi_s V_{ss} \geq V_{max}$). This requires an estimate of the expected maximum base shear demand under the survival level ground motion, V_{max} and the expected minimum shear slip capacity of the base-panel-to-foundation joint, V_{ss}. This is described below.

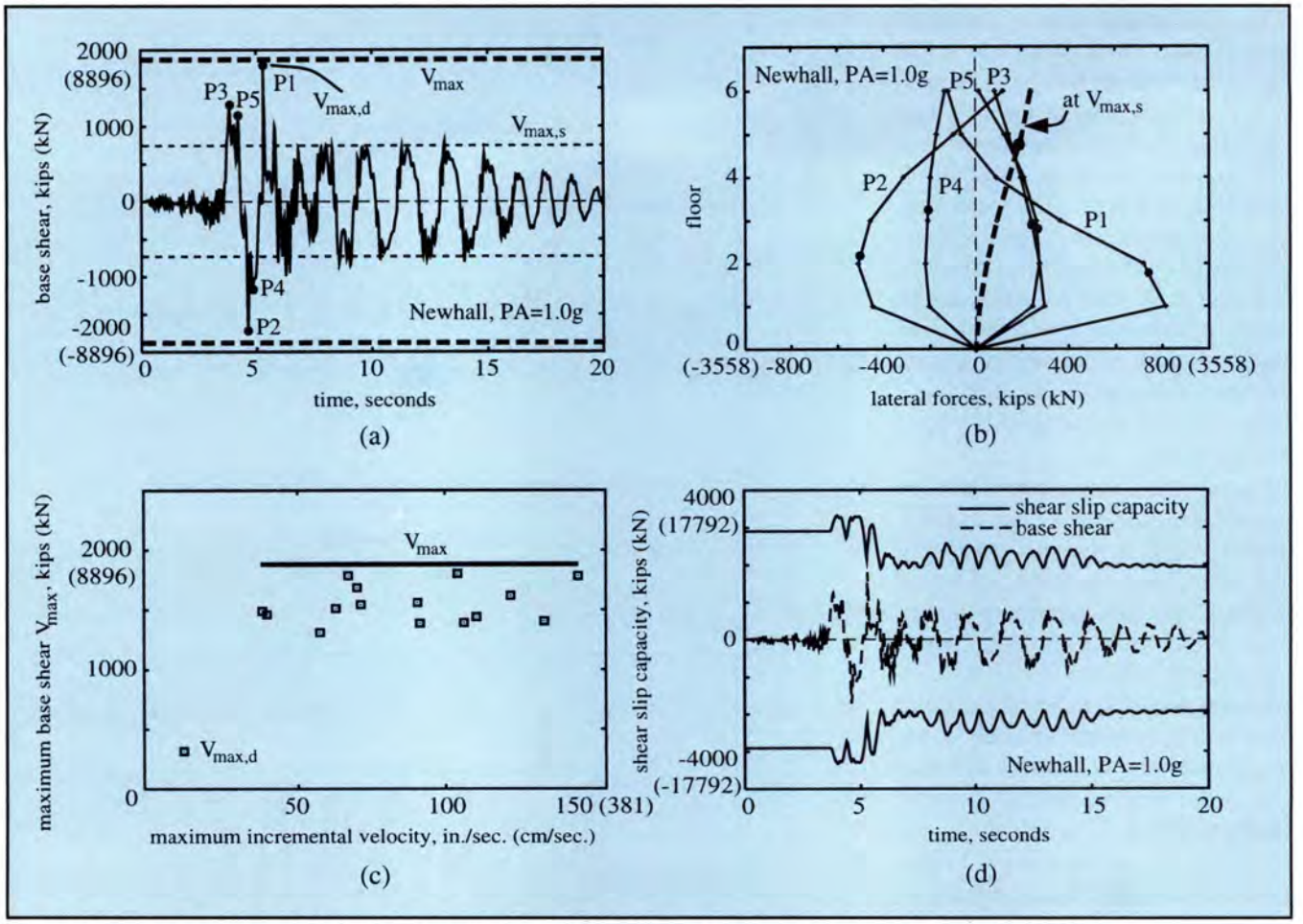

Fig. 12. Shear slip: (a) base-shear time-history; (b) lateral forces; (c) maximum base shear; (d) shear slip capacity.

Expected maximum base shear demand, V_{max} — Fig. 12(a) shows the base shear time-history of Wall WH1 obtained from a nonlinear dynamic time-history analysis under the Newhall ground motion scaled to 1.0*g* to represent a survival level ground motion. The light dashed horizontal lines indicate the maximum base shear reached during a nonlinear static push-over analysis of the wall under combined gravity loads and lateral loads.

In the nonlinear static push-over analysis, the distribution of the lateral loads over the height of the wall is based on the equivalent lateral force procedure in NEHRP.[9] The maximum base shear reached during the static analysis is referred to as the static maximum base shear, $V_{max,s}$, and the maximum base shear reached during the dynamic analysis is referred to as the dynamic maximum base shear, $V_{max,d}$. Fig. 12(a) shows that $V_{max,d}$ is significantly larger than $V_{max,s}$.

Fig. 12(b) shows the lateral inertia forces (i.e., the forces that develop at the floor and roof levels as a result of the acceleration of the floor and roof masses) corresponding to five of the largest peaks on the base-shear time-history shown in Fig. 12(a) (numbered P1 through P5). P1 corresponds to the dynamic maximum base shear, $V_{max,d}$. For comparison, the lateral forces corresponding to $V_{max,s}$ are shown by the dashed line in Fig. 12(b). The location of the resultant of each set of forces is shown by a solid circular marker.

The distribution of the lateral forces corresponding to $V_{max,s}$ is essentially a first mode distribution. The resultant of these forces is located at $0.78h_w$ from the base of the wall, where h_w is the height of the wall. The resultant of the inertia forces corresponding to $V_{max,d}$ (i.e., P1) is located at $0.27h_w$ from the base of the wall (significantly lower than $0.78h_w$). The static maximum base shear, $V_{max,s}$, can be related to the dynamic maximum base shear, $V_{max,d}$, using the base moment capacity of the wall, M_b: $V_{max,s} = M_b / 0.78h_w$ and $V_{max,d} = M_b / 0.27h_w$. Thus, $V_{max,d}$ is roughly 2.9 times $V_{max,s}$. This difference is attributed to the effect of higher modes (with shorter periods and lower resultant heights) which contribute significantly to the inertia forces.

For a wall responding in the nonlinear range, the increase in the base shear demand, V_{max}, due to the higher modes cannot be estimated accurately from a linear-elastic modal analysis procedure such as the one described in NEHRP.[9] This is because the effect of higher modes on the maximum base shear increases significantly due to the nonlinear behavior of the wall. Nonlinear behavior results in a decrease in the lateral stiffness (softening) which results in an elongation of the modal periods. Period elongation often results in an increase in the contribution of the higher modes to the inertia forces. Thus, the contribution of the higher modes to the base shear increases and can be comparable to the contribution of the first mode.

The proposed design approach includes a method to estimate the maximum base shear demand under the survival level ground motion, accounting for the effect of higher modes in the nonlinear range of response.[6] This method is based on a method developed by Kabeyasawa[12] and Aoyama[13] for cast-in-place reinforced concrete walls. The thick dashed horizontal lines in Fig. 12(a) indicate the expected maximum base shear demand, V_{max}, estimated using this method. Fig. 12(c) shows a comparison between V_{max} and the dynamic maximum base shear $V_{max,d}$ obtained from the analyses of Wall WH1 under 15 ground motion records scaled to 1.0g. The horizontal axis of Fig. 12(c) is the maximum incremental velocity of the ground motions. The maximum incremental velocity of a ground motion is equal to the maximum area under the acceleration time-history of the ground motion between two zero crossings. The results indicate that V_{max} provides a good upper bound to $V_{max,d}$.

Shear slip capacity, V_{ss} — The expected minimum shear slip capacity, V_{ss} of an unbonded post-tensioned precast wall is calculated as the product of the coefficient of shear friction, μ along the base-panel-to-foundation joint and the compression force acting through the joint.[6] In the design of the prototype walls, the coefficient of shear friction, μ, was assumed to be 0.7 as specified by the ACI 318 Code[10] for joints between precast members. The compression force acting through the base-panel-to-foundation joint was taken as the sum of the axial force due to gravity and the total post-tensioning steel force.

A minimum total post-tensioning steel force was used to calculate V_{ss} considering a reduction in the initial total post-tensioning steel force (i.e., prestress) due to the inelastic straining of the steel. The minimum total post-tensioning steel force was calculated assuming that the wall displaces, in both directions, to Δ_{sur}. This is described in more detail by Kurama et al.[6]

Fig 12(d) shows the shear-slip capacity time-history (solid lines) of Wall WH1 under the Newhall ground motion scaled to 1.0g. The shear slip capacity time-history is calculated using $\phi_s\mu = 0.6$. The shear slip capacity varies during the ground motion because the total post-tensioning steel force varies as shown in Fig. 11(a). The minimum shear slip capacity is reached when the minimum total post-tensioning steel force is reached. The dashed line in Fig. 12(d) shows the base-shear time-history of the wall [the same with Fig. 12(a)]. The most critical time for shear slip occurs at around 6 seconds when the maximum base shear, $V_{max,d}$, is reached just before the minimum shear slip capacity is reached. At this time, the shear slip capacity exceeds the base shear indicating that shear slip does not occur.

It is noted that additional work on the estimation of the shear slip capacity is needed. The coefficient of shear friction of the base-panel-to-foundation joint in an unbonded post-tensioned precast wall may be smaller than 0.7 as a result of the high compression stresses that occur in the joint due to post-tensioning and gap opening. Furthermore, the shear slip capacity of the joint may degrade under cyclic loading. Therefore, it is recommended that a conservative value of the coefficient of shear friction be used in design.

CURRENT RESEARCH

Currently, a large-scale experimental evaluation of the lateral load behavior of unbonded post-tensioned precast walls is being conducted at Lehigh University. Nine half-scale six-story wall specimens are being tested under combined gravity loading and cyclic lateral loading. Based on the results of these tests, the lateral load behavior of the walls will be evaluated and the shear slip capacity of the walls will be quantified.

The current research at the Leheigh University is funded by the National Science Foundation under Grant No. CMS-9612165, with substantial support from the precast concrete industry which has donated the test specimens and test fixtures, and has provided technical support for the design of the test specimens.

More recently, an analytical investigation of the effect of large openings (in the wall panels) on the seismic behavior and design of unbonded post-tensioned precast walls has been initiated at the University of Notre Dame. The openings can accommodate doors, windows, and mechanical penetrations which may be needed due to architectural or functional requirements.

The current research at the University of Notre Dame is funded in part by the Precast/Prestressed Concrete Institute by a 1998-1999 Daniel P. Jenny Research Fellowship. Detailed finite element models of the walls are being developed using the ABAQUS program. These models will be verified based on experimental results obtained at Lehigh University and will be used to investigate the effect of large openings in the walls.

CONCLUSIONS

The research summarized in this paper shows that unbonded post-tensioned precast walls provide a feasible alternative to conventional monolithic cast-in-place concrete walls in seismic regions. Conclusions regarding the seismic behavior and design of the walls are presented below.

1. Unbonded post-tensioned precast walls have the ability to soften and undergo large nonlinear lateral drift with little damage. As a result, only minor repair to the walls may be needed after a design level ground motion.

2. The nonlinear drift occurs primarily due to the opening of gaps along the horizontal joints.

3. Because little damage occurs in the walls, the behavior of the walls under cyclic lateral load is nearly nonlinear-elastic.

4. Unbonded post-tensioned precast walls can be designed to resist design level ground motions with little damage, and to resist severe survival level ground motions with damage, but without collapse. Design guidelines and requirements to obtain this behavior are presented in the paper.

5. Accurate estimates of the maximum lateral drift demands under design level and survival level ground motions are needed for design. The method used to estimate the maximum drift demands in the proposed design approach needs to be improved.

6. Nonlinear dynamic time-history analyses show that, as a result of the

nearly nonlinear-elastic behavior, an unbonded post-tensioned precast concrete wall has larger lateral drift under earthquake loading than a comparable cast-in-place reinforced concrete wall. However, an unbonded post-tensioned precast wall has significantly smaller residual drift (at the end of the ground motion) than a cast-in-place wall.

7. Shear slip along the horizontal joints is not a desired mode of lateral displacement. Shear slip under severe survival level ground motions can be prevented using the proposed design approach.

8. Inelastic straining of the post-tensioning steel during a ground motion results in a reduction in the total post-tensioning steel force. This reduction significantly affects the hysteretic behavior of the walls and results in a reduction in the shear slip capacity. The design approach includes a method to estimate the reduction in the total post-tensioning steel force under survival level ground motions.

RECOMMENDATIONS

Preliminary design recommendations are described in the paper. These include recommendations regarding the selection of the wall design properties (e.g., initial stress in the post-tensioning steel, total area of the post-tensioning steel, wall length, unbonded length of the post-tensioning steel, location of the post-tensioning steel, amount of spiral reinforcement) to achieve the design capacities as required by the proposed design approach. Design examples and more comprehensive design recommendations are expected to be developed based on the current experimental and analytical research.

The dynamic analysis results indicate that the equal displacement assumption can be used to estimate the maximum roof drift demands for walls designed for sites with a stiff soil profile but not for sites with medium or soft soil profiles. Improved methods to estimate the maximum roof drift demands for sites with medium and soft soil profiles are expected to be developed and incorporated into the proposed design approach based on current research.

Shear slip along the horizontal joints is prevented by requiring that the minimum shear slip capacity of the base-panel-to-foundation joint is larger than the maximum base shear demand. The paper proposes a method to estimate the maximum base shear demand including the effect of higher modes, and a method to estimate the minimum shear slip capacity including the reduction in prestress due to inelastic straining of the post-tensioning steel. It is recommended that a conservative value of the coefficient of shear friction be used in design. Further recommendations regarding the shear slip capacity are expected to be developed based on the current experimental research.

ACKNOWLEDGMENTS

The investigation was funded by the National Science Foundation (NSF) under Grant No. BCS-9307880 as part of the PREcast Seismic Structural Systems (PRESSS) research program. The support of the NSF Program Director Dr. S. C. Liu and Program Coordinator Dr. M. J. N. Priestley is gratefully acknowledged.

The authors also wish to thank several individuals for their assistance in the conduct of this work: K. Baur, High Concrete Structures, Inc.; M. Bertolini, Blakeslee Prestress, Inc.; N. Cleland, Blue Ridge Design, Inc.; T. D'Arcy, The Consulting Engineers Group, Inc.; H. Gleich, Metromont Materials Corporation; P. Johal, Precast/Prestressed Concrete Institute; S. Nakaki, Englekirk and Nakaki, Inc; H. Wilden, H. Wilden & Associates, Inc.; K. Jacob and N. Barstow, Lamont-Doherty Geological Observatory.

The authors appreciate the thoughtful comments provided by the reviewers. The opinions, findings, and conclusions expressed in the paper are those of the authors and do not necessarily reflect the views of the NSF or the individuals and organizations acknowledged above.

REFERENCES

1. Mueller, P., "Experimental Investigation on the Seismic Performance of Precast Walls," Ninth World Conference on Earthquake Engineering, Tokyo-Kyoto, Japan, V. IV, 1988, pp. 755-760.
2. Oliva, M., Clough, R., and Malhas, F., "Seismic Behavior of Large Panel Precast Concrete Walls: Analysis and Experiment," PCI JOURNAL, V. 34, No. 5, September-October 1989, pp. 42-66.
3. Hutchinson, R., Rizkalla, S., Lau, M., and Heuvel, S., "Horizontal Post-Tensioned Connections for Precast Concrete Load-bearing Shear Wall Panels," PCI JOURNAL, V. 36, No. 6, November-December 1991, pp. 64-76.
4. Priestley, M.J.N., "Overview of PRESSS Research Program," PCI JOURNAL, V. 36, No. 4, July-August 1991, pp. 50-57.
5. Kurama, Y., Pessiki, S., Sause, R., Lu, L.W., and El-Sheikh, M., "Analytical Modeling and Lateral Load Behavior of Unbonded Post-Tensioned Precast Concrete Walls," Research Report No. EQ-96-02, Department of Civil and Environmental Engineering, Lehigh University, Bethlehem, PA, November 1996, 191 pp.
6. Kurama, Y., Sause, R., Pessiki, S., Lu, L.W., and El-Sheikh, M., "Seismic Design and Response Evaluation of Unbonded Post-Tensioned Precast Concrete Walls," Research Report No. EQ-97-01, Department of Civil and Environmental Engineering, Lehigh University, Bethlehem, PA, November 1997, 184 pp.
7. Allen, M., and Kurama, Y., "Lateral Load Behavior and Design of Unbonded Post-Tensioned Precast Walls with Large Openings," in preparation for submittal to the PCI JOURNAL, 1999.
8. El-Sheikh, M., Sause, R., Pessiki, S., and Lu, L.W., "Seismic Behavior and Design of Unbonded Post-Tensioned Precast Frames," PCI JOURNAL, V. 44, No. 3, May-June 1999.
9. Building Seismic Safety Council, "NEHRP Recommended Provisions for the Development of Seismic Regulations for New Buildings," BSSC, Washington, D.C., 1991, 1994, 1997.
10. ACI Committee 318, "Building Code Requirements for Structural Concrete (ACI 318-95) and Commentary (ACI 318R-95)," American Concrete Institute, Farmington Hills, MI, 1995, 369 pp.

11. Nassar, A., and Krawinkler, H., "Seismic Demands for SDOF and MDOF Systems," Report No. 95, Department of Civil Engineering, Stanford University, CA, June 1991, 204 pp.
12. Kabeyasawa, T., "Ultimate-State Design of Wall-Frame Structures," in *Earthquake Resistance of Reinforced Concrete Structures*, A Volume Honoring Hiroyuki Aoyama, Editor: T. Okada, Department of Architecture, Faculty of Engineering, University of Tokyo, Japan, November 1993, pp. 431-440.
13. Aoyama, H., "Earthquake Resistant Design of Reinforced Concrete Frame Buildings with Flexural Walls," in *Earthquake Resistance of Reinforced Concrete Structures*, A Volume Honoring Hiroyuki Aoyama, Editor: T. Okada, Department of Architecture, Faculty of Engineering, University of Tokyo, Japan, November 1993, pp. 78-100.

APPENDIX – NOTATION

a_p = area of one post-tensioning bar
A_p = total area of post-tensioning steel in cross section
f_c' = compressive strength of unconfined concrete
f_{pi} = initial stress in post-tensioning steel
f_{pu} = ultimate strength of post-tensioning steel
g = acceleration due to gravity
G = amount of axial force at base of wall due to gravity load
h_w = wall height
l_{unb} = unbonded length of post-tensioning steel
l_w = wall length
M_b = base moment capacity
P_i = total post-tensioning force
Q_{des} = linear-elastic base shear demand for design level ground motion
Q_{sur} = linear-elastic base shear demand for survival level ground motion
R = response modification coefficient (R = 4.5)
t_w = wall thickness
V_{csc} = base shear capacity at failure state
V_{dec} = base shear capacity at decompression state
V_{des} = design base shear demand
V_{ell} = base shear capacity at softening state
V_{llp} = base shear capacity at yielding state
V_{max} = expected maximum base shear demand
$V_{max,d}$ = maximum base shear reached during nonlinear dynamic time-history analysis
$V_{max,s}$ = maximum base shear reached during nonlinear static push-over analysis
V_{ss} = expected minimum shear slip capacity
δ_{all} = allowable story drift under design level ground motion
δ_{des} = expected maximum story drift demand under design level ground motion
Δ_{csc} = roof drift capacity at failure state
Δ_{ctc} = roof drift capacity corresponding to crushing of concrete inside wire mesh
Δ_{dec} = roof drift capacity at decompression state
Δ_{des} = expected maximum roof drift demand under design level ground motion
Δ_{ell} = roof drift capacity at softening state
Δ_g = maximum roof drift that can be sustained by gravity load system
Δ_{llp} = roof drift capacity at yielding state
Δ_{sur} = expected maximum roof drift demand under survival level ground motion
ρ_{sp} = ratio of volume of spiral reinforcement to volume of confined concrete
ϕ_f = capacity reduction factor for combined axial compression and flexure (ϕ_f = 0.75)
ϕ_s = capacity reduction factor for shear (ϕ_s = 0.85)